Journal of Physics: Conference Series

PAPER • OPEN ACCESS

Improvement of Electric Aircraft Endurance through Propeller Optimization via BEM-CFD Methodology

To cite this article: José D Hoyos *et al* 2021 *J. Phys.: Conf. Ser.* **1733** 012011

Journal of Physics: Conference Series **1733** (2021) 012011 doi:10.1088/1742-6596/1733/1/012011

Improvement of Electric Aircraft Endurance through Propeller Optimization via BEM-CFD Methodology

José D Hoyos[1], Jesús H Jímenez[1] and Pablo Alvarado[1]
[1]Aeronautical Engineering Faculty, Universidad Pontificia Bolivariana (050031), Medellín, Colombia.

Email: jose.hoyos@upb.edu.co; jhernan.jimenezg@gmail.com; juan.alvarado@upb.edu.co

Abstract. An exhaustive optimization method is developed to minimize the power consumption for a propeller-driven electrical aircraft. The method finds the optimal value for a wide range of geometrical and operational parameters for a target thrust and airspeed. The optimization routine employs BEM for propeller predictions fed with aerodynamic airfoil data obtained from a proposed combined CFD-Montgomerie method which is also validated, furthermore several corrections to account for compressibility, three dimensional, viscous and Reynolds number effects are implemented. This BEM model showed an adequate fitting with experimental data. Additionally, Goldstein optimization via Vortex Theory is employed to design pitch and chord distributions minimizing the induced losses of the propeller. The optimization algorithm is validated through a study case where an existent optimization problem is approached leading to very similar results. Some trends and insights are obtained and discussed from the study case regarding the design of an optimal propulsion system. Finally, CFD simulations of the study case are carried out showing a slight relative error of BEM.

1. Introduction

The main purpose of this work is to present a methodology to design an optimal propeller to reduce the energy consumption given a target condition such as cruise or loiter, for a certain electric aircraft. Additionally, trends and insights into the interaction of the variables in the whole electric propulsion system are investigated. This research seeks to expand and contribute in different ways: present a high fidelity Computational Fluid Dynamics (CFD) method coupled with a known extrapolation model to predict the airfoil performance in order to get more suitable Blade Element Momentum Theory (BEM) results, implement a computational code of BEM with several corrections to capture appropriately some propeller phenomena including the change in performance related to Reynolds number, viscosity, compressibility, and three-dimensional effects, and finally, design an optimization algorithm for a motor-propeller system to reduce the energy consumption for specific design conditions, which can also be extended to a multi-objective optimization for any kind of propeller-driven aircraft.

Commonly, numerical potential theory via panel methods, such as XFOIL, are implemented into the BEM algorithm to predict the aerodynamic coefficients [1, 2]. Although it makes good approaches with a low computational cost, low Reynolds conditions, the stall point and the post-stall regime are not well predicted; furthermore, XFOIL overpredicts maximum lift coefficient and underpredicts minimum drag [3]. On the other hand, CFD methods have demonstrated more reliable results than XFOIL [4, 5], especially in the non-linear regime and low Reynolds conditions as long as a proper turbulence model and mesh are employed. Considering that correct BEM predictions decisively depend on the airfoil performance data [6], CFD methods are adopted to predict the airfoil linear and stall point; then, in order to keep a relatively low computational cost, the post-stall region is approximated through the Montgomerie extrapolation method [7].

The problem aims to reduce the energy consumption for an electric propeller-driven aircraft in order to maximize its range and endurance through the design of an optimal propeller for this purpose. The model requires a known motor, a certain target cruise speed, V_∞, an altitude, and a desired target thrust, T. Thus, the optimization method finds the optimal geometric parameters of the propeller such as chord, c and pitch distributions, airfoil for each blade section (selected from a known airfoil database), propeller diameter, d and the number of blades, B to finally find the operating rotational speed, Ω at which energy consumption is minimized fulfilling the target thrust. Some constraints are applied: the maximum motor power can not be exceeded, there is a maximum propeller diameter, d_{max} and the maximum voltage can not be exceeded either. The work builds on previous research on the use of the BEM with corrections for aircraft propellers [1], the use of CFD to obtain the aerodynamic data that feeds the BEM and CFD of the 3D propeller [8], as well as optimization results in propellers [9, 10, 11].

2. Electric propulsion model

There are some definitions in propeller metrics derived by a dimensional analysis [12, pp. 566–568], which are the advance ratio, J (equation (1)) used to quantify the effects on forward motion and rotational speed, the thrust coefficient, C_T and torque coefficient, C_Q.

$$J = \frac{V_\infty}{nd} \qquad (1) \qquad\qquad C_T = \frac{T}{\rho n^2 d^4} \qquad (2) \qquad\qquad C_Q = \frac{Q}{\rho n^2 d^5} \qquad (3)$$

Where n is the rotational speed in revolutions per second, ρ is the air density and Q the shaft torque. Using the usual circuit equations and the conservation of energy, the fundamental relationships for the Direct Current (DC) electric motor can be deducted, as shown from equation (4) to equation (6) including the Electronic Speed Controller (ESC) resistance in the model.

$$Q(i) = (i - i_o)K_Q \qquad (4) \qquad\qquad v_m(\Omega) = \frac{\Omega}{K_V} \qquad (5)$$

$$v(i, \Omega) = v_m(\Omega) + i(R_a + R_{ESC}) = \frac{\Omega}{K_V} + i(R_a + R_{ESC}) \qquad (6)$$

With i the current, i_o the no-load current, K_Q the motor torque constant, K_V the motor speed constant, v_m the back electromotive force, v the electric motor voltage, R_a the motor electrical resistance and R_{ESC} the Electronic Speed Controller resistance. For an electrical propulsion system there are mainly two efficiencies (ESC efficiency also has an impact in total efficiency, nevertheless, it approaches 1 at high PWM frequencies or high power, see [13] for further information) that must be considered: the electrical efficiency, η_E that correlates the mechanical power developed in the motor, P_S and the power delivered from the battery, P_E (equation (7)), and the propeller efficiency, η_P that correlates the power delivered to the flowing air mass and the power required to drive the propeller (equation (8)). Both efficiencies result in the total efficiency, η_T (equation (9)) [1, p. 4].

Journal of Physics: Conference Series **1733** (2021) 012011 doi:10.1088/1742-6596/1733/1/012011

$$\eta_E \equiv \frac{P_S}{P_E} = \frac{Q\Omega}{vi} \quad (7) \qquad \eta_P = \frac{1}{2\pi}\frac{C_T}{C_Q}J \quad (8) \qquad \eta_T \equiv \eta_E \eta_P \quad (9)$$

3. BEM Model

3.1 Modeling Overview

The Blade Element Momentum Theory uses both Blade Element Theory and One-dimensional Momentum Theory in order to calculate through an iterative process the induced velocities (represented by the induction factors) on each station of a discretized blade. The Blade Element Theory deals with relative velocities and angles while the Momentum Theory deals with the relationship between velocities at different points of the flow. A detailed description of both methods is presented by Glauert in [14]. The method divides the blade into discrete independent elements with an associated airfoil from which lift and drag coefficients can be computed for the correspondent angle of attack. Lift and drag forces are decomposed on normal and tangential which can be integrated to compute total thrust, torque and power.

3.2 Corrections

Lift and drag polars are obtained from CFD simulations and extrapolated through the Montgomerie method, however, the CFD simulations should be done at specific conditions, that is, specific Reynolds number; then the drag coefficient is corrected to account for the effect of Reynolds number; the correction is proposed on [15]. Lift coefficient is not corrected; the linear part of the lift curve does not considerably change with Reynolds. The stall region is affected but a Reynolds correction for this has not been developed so far. An approximated method to calculate Prandtl's tip-loss factor on each section of a rotor is presented on [16]; this method developed for wind turbines is also valid for propellers. The hub-loss correction factor also presented on [16] is very similar to the tip-loss correction factor. Finally, to account for tip and hub losses, both correction factors are multiplied to obtain the final correction factor to be applied at the loads of each blade station. The rotational effects are associated to the three-dimensionality of the problem. An approach to correct the 2D lift data is shown in [17], see equation (10), where the value of the coefficient b is 3.1 for rotors; but for this study, the factor takes a value of 1.5 as it was selected by McCrink on [1, p. 3] being a more similar work.

$$c_{l_{3D}} = c_{l_{2D}} + b\left(\frac{c}{r}\right)^2 \left(c_{l_{pot}} - c_{l_{2D}}\right)\left(\frac{\Omega r}{V_{rel}}\right)^2 \quad (10)$$

Where V_{rel} is the relative velocity, $c_{l_{3D}}$ the 3-D corrected lift coefficient, $c_{l_{2D}}$ the uncorrected lift coefficient and r the local radius. Note that the term $c_{l_{pot}} - c_{l_{2D}}$ accounts for the stall effects on the correction, being the difference between the lift coefficient calculated through potential flow c_{lpot} and the estimated 2-D lift coefficient. Lift and drag coefficients feeding the BEM method are corrected to account for compressibility effects through the Karman-Tsien correction [18].

4. Combined BEM-CFD

4.1 Turbulence model selection

In the wide range of RANS models available, the Transition SST model is selected. It is a four-equation turbulence model based on SST $k-\omega$ model, additionally, two other equations are added: one for the intermittency, γ and other for the laminar-turbulent transition with $Re_{\theta t}$ criteria, which links empirical transition data with intermittency equation [19]. This four-equation model is also termed as the $\gamma - Re_\theta-$SST model, which is commonly used due to its reliable results for linear and stall regime including low Reynolds number condition [20, 21].

4.2 Grid convergence and simulation settings

The domain is a structured circle (the structured mesh is built in Pointwise® software) which has a radius of 100 chords. This kind of o-ring grid type allows the use of only one mesh for all the angles of attack, it is achieved varying the flow direction at the inlet which is the external circumference, such is carried out in [5, 21]. The airfoil is defined as a wall. The distance from the airfoil to the first layer is calculated by flat-plate boundary layer theory as $8.524 \cdot 10^{-5}$ m for the three meshes with the aim of keeping the non-dimensional wall distance, $y^+ = 1$ at this location, it is recommended for more reliable CFD turbulent predictions.

The airfoil tested is a NACA4412 at a Reynolds number (Re) of 250000. The simulations are performed using ANSYS FLUENT® steady-state solver. A density-based solver is applied. The external circumference is defined as pressure far-field with a mach number of 0.01074, this kind of boundary requires an ideal gas law to be implemented. A second-order upwind (SOU) scheme is used for spatial discretization for flow, turbulence, and momentum equations [5, p. 210]. The conservative equations are solved by implicit formulation and Advection Upstream Splitting Method (AUSM) flux type, finally, the pseudo transient option is implemented with a 0.001 timescale factor to achieve fast convergence. The maximum lift coefficient of the medium refinement mesh was calculated as 1.34 compared to the 1.15 and the 1.33 of the coarse and fine mesh respectively, the medium refinement mesh with 25578 cells and a growth rate of 1.1 with 200 points along the airfoil is selected to run the simulations due to its low difference in the maximum lift coefficient prediction compared to the fine mesh.

4.3 CFD-Montgomerie validation

An airfoil NACA0012 with Re of 360000 is selected to validate the aerodynamic predictions of the CFD-Montgomerie methodology, where the transition between CFD and Montgomerie approaches occurs at an angle of attack of 10°, which is the stall angle predicted by CFD at the tested conditions.

From the results obtained, the drag and lift coefficient estimations have a Mean Absolute Percentage Error (MAPE) of 22.98% and 16.55% respectively, this does not represent a critical problem since the pre-stall regime shows a lift MAPE of 4.43% and most of the airfoils on the blade lie on this regime.

5. Propulsion model validation

The BEM-CFD model proposed before is validated through a comparison against estimated manufacturer APC data [22] which employs vortex theory for propeller performance and the NASA Transonic Airfoil (TAIR) [23] code to generate estimations for sections lift and drag. Moreover, an experimental data comparison is also performed using data from the UIUC database [24]. The APC 10x7E Propeller is selected for the comparison, which is geometrically approximated by S8037 airfoil from hub to 50% of radius length, NACA 4412 the next 25% and Clark-Y airfoil until tip ([25, p. 26]). The C_T vs J graphs comparison is shown in figure 1a while η_P vs J graphs comparison is shown in figure 1b. From the data shown in figure 1, the MAPE in comparison with experimental data is calculated for both $C_T(J)$ and $\eta_P(J)$ data as 9.45% and 11.12% respectively.

6. Optimization algorithm

6.1 Chord and pitch distribution

Prandtl and Betz developed a Vortex Theory applied to propellers [26], analog to the wing's lifting line theory. The vortex theory models the wake that the propeller sheds as a helical vortex sheet which induces velocities along the blades changing the local angle of attack of each blade section [27]. The theory states that there is a pitch and chord distribution that accomplishes the constant horizontal velocity on each helical wake which minimizes the loss of kinetic energy (induced drag). The method for the estimation of such distribution developed by Prandtl and Betz was improved

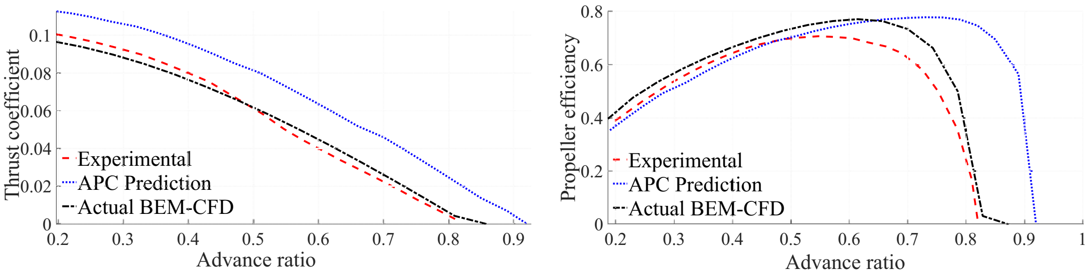

(a) $J\ vs\ C_T$ comparison

(b) $J\ vs\ \eta_P$ comparison

Figure 1. Performance results comparison for 10x7E APC propeller.

by Goldstein [28], and this is the method selected to find the optimal pitch and chord distributions for the optimization algorithm.

6.2 Airfoils selection

The optimization algorithm evaluates a list of airfoils along the propeller, which are selected taking into account the kind of airfoil employed for each section of a small propeller [25, 29, 30]. The airfoil along the propeller varies. At the root there is a low Reynolds airfoil with a strong camber, while at the tip a less cambered airfoil is employed [14], this decrement in camber along the radius is implemented due to structural criteria. Once the camber filter is carried out, the criterion to select the airfoils is the best lift-drag ratio called aerodynamic efficiency estimated from [30]. Tree different airfoils for 3 different sections of the blade (root, mid and tip) are selected for the optimization process. Root airfoils are MH112, FX-MP-160 and E591, middle airfoils are MH 115, HS1712 and NACA 4412, tip airfoils are GOE 796, MH122, SD7037. The Reynolds number at which airfoil data is going to be obtained by CFD for tip, middle, and root airfoil simulations is selected as 530000, 130000, and 90000 respectively.

6.3 Algorithm overview

The algorithm has three main subroutines implemented: the Goldstein optimization, the BEM algorithm, and the electric motor model. The first step in the optimization algorithm is to set the design parameters and the range for the variables to optimize, which are both inputs for Goldstein and BEM methods: cruise speed, a certain flight altitude that allows the calculation of air density, sound speed, and viscosity through the standard atmosphere and Sutherland's law, target thrust, the number of blade sections, and the range for the design variables such as diameter, the number of blades, and the guessing rotational speed, Ω_{guess}, which is a guess value for the Vortex algorithm that is different from Ω due to the slight discrepancy between Vortex and BEM predictions. Finally, root, mid, and tip airfoils are selected from the list mentioned in the previous subsection, the position of the middle airfoil is also varied for the optimization. Additionally, the lift and drag coefficients are linearly interpolated between the known airfoils performance estimated from the CFD-Montgomerie method in order to account for the shape transition.

The next step is the Goldstein optimization whose outputs are the optimal chord and pitch distributions for the design conditions, including the Ω_{guess}. Then, the BEM algorithm employs this data to calculate the propeller performance, whose useful outputs are the thrust and torque as function of rotational speed and $\eta_P(J)$. In this step, the rotational speed at which the target thrust is achieved is found, subsequently, the operational advance ratio is calculated taking into account the estimated rotational speed to finally obtain the propulsive efficiency.

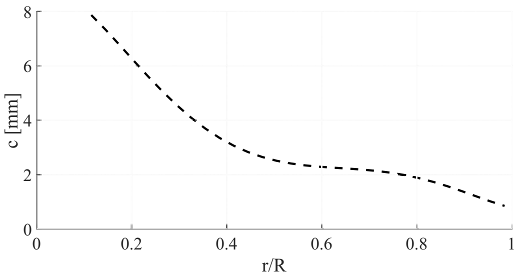

(a) Chord distribution.

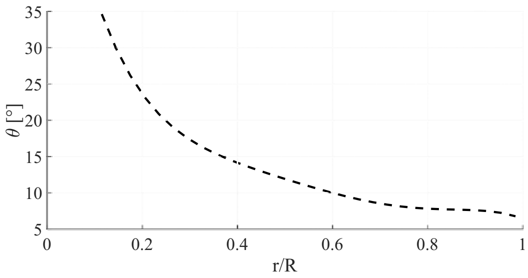

(b) Pitch distribution.

Figure 2. Propeller optimal chord and pitch distribution case.

Finally, the electric inputs i_o, K_V, R_a and R_{ESC} are employed for the DC electric motor model. The torque is calculated from equation (8), then the current consumption is found from equation (4) and the voltage from equation (6). The electric performance is summarized by i, v, η_E calculated from equation (7), and η_T from equation (9). Some constraints are applied to discard the solutions that exceed the maximum allowable power and voltage of the motor. Additionally, there is another internal constraint to restrict the propeller tip speed to Mach 0.7 (as used in [10, p. 1344]), with the aim of assuring that sound speed is not exceeded at any point over the airfoil. The solution with the minimum electrical power consumption, P_E, is selected as the optimal design point to maximize endurance.

7. Optimization validation

7.1 Optimization case

The optimization results are validated through a comparison with an existent optimization case presented in [9] at sea level, which main data and constraints are the following: $R_a = 0.1\Omega$, $K_V = 222.22\frac{rad}{Vs}$, $d_{max} = 0.3m$, $T = 3.5N$, $V_\infty = 10\frac{m}{s}$. In addition to this data, the algorithm is tested for a two and three-bladed propeller with a hub radius of 10% of the total blade radius and a no-load current of 0 A. The range to test the diameter is from 0.1m to 0.3m divided in 20 steps, Ω_{guess} in 25 steps from the value corresponding to J=1 to the one correspondent to 0.7M at the blade tip, finally the position for the middle airfoil is tested from 40% to 70% of radius length with 3 steps. The results of the optimal propeller parameters and the electric performance are shown in table 1.

Table 1. Study case optimal propeller performance

d [m]	Ω [$\frac{rad}{s}$]	i [A]	η_P	η_E	η_T	B	$P_S[W]$	$P_E[W]$	Root	Middle	Tip
0.262	1447.7	8.48	63.35%	88.38%	55.99%	2	55.24	62.51	E591	MH115	MH122

The optimal propeller designed in [9] theoretically achieved a power consumption of $P_E = 56$ W. The current design predicts a minimum energy consumption of $P_E = 62.51$ W with different values for variables as d, Ω, and chord and pitch distributions shown in figure 2a and figure 2b, respectively. The airfoils selected by the algorithm are those with the highest aerodynamic efficiency due to the model does not take into account the structural stresses.

From the cases generated by the algorithm some important trends related to power consumption are studied. The main tendency shows that, for a given target thrust, an increase in propeller diameter and operational rotational speed results in lower power consumption due to their conse-

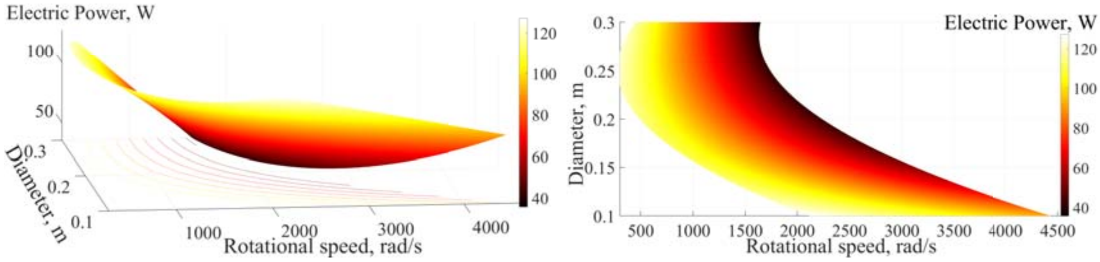

(a) Surface plot **(b)** Heat map

Figure 3. Impact of d and Ω in P_E.

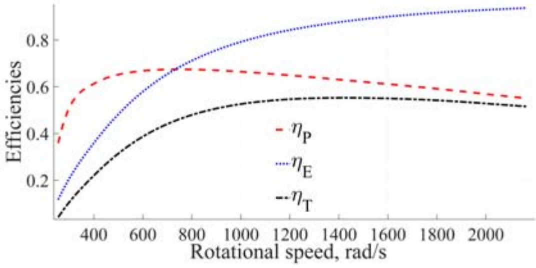

Figure 4. η_P, η_E and η_T for different design rotational speeds ($d = 0.262$ m, $B = 2$).

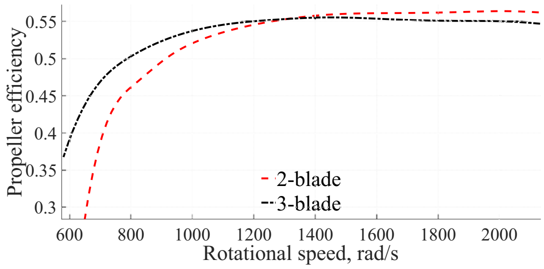

Figure 5. η_P at different operational rotational speed for 2 and 3 blades ($d = 0.17$ m).

quent increment of tangential speed, resulting in a higher operational Reynolds number, condition which improves the aerodynamic efficiency of section airfoils. The tendency is shown in figure 3 done for a two-bladed propeller with the airfoils selected for the optimal case described in table 1.

Additionally, for different generated cases, the behavior of propulsive, electric, and total operational efficiency is analyzed for a specific range of rotational speeds, as shown in figure 4. The data shows how the optimal operational condition for the propeller (the point with the highest η_P) is not close to the optimal motor operational point of η_E. The trend shows that the motor achieves higher values of electric efficiency at high values of rotational speed. On the other hand, the efficiency peak of the propeller is achieved at a different value of rotational speed, that is the main reason to use a gearbox for this kind of systems.

From the study case, a tendency chart is built to show how the number of blades affects the operational propulsive efficiency at different operational rotational speeds as shown in figure 5. It is shown that for high rotational speeds, higher efficiencies can be reached because of the higher operational Reynolds of the whole blade and its positive effect on airfoil performance; additionally, the tendency shows that, for fixed diameter, there is an advantage in using a 3-blade propeller at low and moderate rotational speeds, this advantage is more marked for lower rotational speeds. A 2-blade propeller shows better performance at higher rotational speeds.

7.2 CFD Comparison

To evaluate the performance of the optimal propeller designed in the case of the study presented before, numerical analyses are performed by using Autodesk® CFD software, which employs the finite element method for the discretization. It is intended to compare the reliability and validity of the BEM method with CFD results. The simulation employs a rotatory region which is a

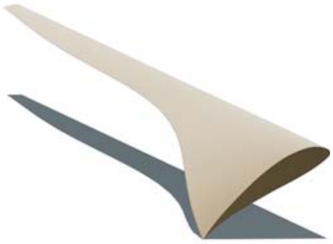

(a) Optimal blade 3D model.

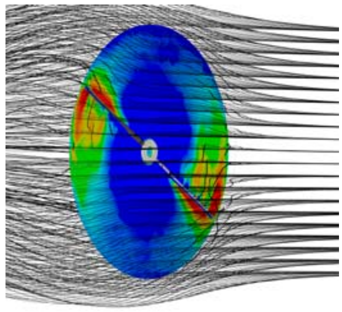

(b) Propeller flow interaction.

Figure 6. Optimal propeller CFD study.

cylindrical-shaped region around the propeller. The external boundary has the velocity inlet boundary with $10\ m/s$ and the outlet face with $0\ Pa$ gauge pressure. A structured quadrilateral mesh of 15 layers is employed along the blade surface with a growth rate of 1.2. The total number of fluid and solid elements are 7095368 and 281024, respectively. The selected model for turbulent flow is the SST k-ω, and a time step of 0.00005 s with 20 inner iterations is employed. The result shows a total force T= 3.40 N in the two blades, without taking into account the hub drag which is not predicted in the BEM method. the relative error of the prediction presents a relative error of 2.94 %.

8. Conclusions

The high fidelity CFD airfoil data extrapolated from stall through Montgomerie method showed a suitable balance between accuracy and computational cost. The set of improvements for the basic BEM model capture a wide range of operational conditions and physical effects, showing a well fitting to experimental data and excellent agreement with CFD propeller results.

Besides the operational rotational speed, the energy consumption of the propulsion system showed to be affected by the propeller diameter, showing further dependency on Reynolds number. It was evident how larger blades operating at high rotational speeds showed to be more effective because the relatively high operational Reynolds of the blade benefits the airfoil performance, however, there are some limitations such as the fact the increment on rotational speeds may cause the tip of the blades to reach the speed of sound spoiling its performance.

The electric efficiency showed to be higher when the propeller operates at high rotational speeds, however, the propulsive efficiency has a different peak depending on the propeller design, hence the total efficiency, which directly affects the power consumption, presents a peak between them, being a trade-off on the optimal propeller and electric system operation. It suggests a change in the K_V motor constant or the employ of a gear ratio to match both electric and propeller peak efficiency. Additionally the trend analysis showed how the number of blades impacts the overall performance of the propulsion system depending on the operational condition; keeping the propeller diameter fixed, the three-blade propeller performed better at low operational rotational speeds, while for higher values the two-blades propeller showed higher performance.

From both CFD propeller simulation and experimental comparison it is concluded that the algorithm yields a slightly optimistic prediction of thrust due to the limitations of BEM, which does not properly reflect the effects of the wake. Moreover, the inaccuracies inherent in the CFD, BEM, and applied corrections also have an undesirable impact on the predictions.

The propeller thrust predictions done by the presented methodology have a higher fitting with experimental data than the torque results, which shows to be underestimated. Hence the total efficiency tends to be overestimated. There are two main reasons for it, both due to the fact that torque is strongly related to drag. The first reason is the higher relative error in CFD-Montgomerie drag prediction in comparison with the lift one. The second reason is that the drag coefficient is markedly dependent on the Reynolds number, causing the results obtained from CFD to have an appreciable error due to the different final operating conditions in spite of the Reynolds number correction employed, which is just a coarse approach.

References

[1] Matthew Mccrink and James Gregory. Blade element momentum modeling of low-reynolds electric propulsion systems. *Journal of Aircraft*, 54:1–14, 07 2016. doi: 10.2514/1.C033622.
[2] David Lee Wall. Optimum propeller design for electric uavs. Master's thesis, Auburn University, 2012.
[3] J. G. Coder and M. D. Maughmer. Comparisons of theoretical methods for predicting airfoil aerodynamic characteristics. *Journal of Aircraft*, 51(1):183–191, 2014.
[4] R. Barrett and A. Ning. Comparison of airfoil precomputational analysis methods for optimization of wind turbine blades. *IEEE Transactions on Sustainable Energy*, 7(3):1081–1088, 2016. doi: 10.1109/TSTE.2016.2522381.
[5] J. Morgado, R. Vizinho, M.A.R. Silvestre, and J.C. Páscoa. Xfoil vs cfd performance predictions for high lift low reynolds number airfoils. *Aerospace Science and Technology*, 52: 207–214, 2016. ISSN 1270-9638. doi: 10.1016/j.ast.2016.02.031.
[6] L. Danielle Koch. Design and Performance Calculations of a Propeller for Very High Altitude Flight. Technical report, NASA/TM—1998-206637, 02 1998. URL `https://ntrs.nasa.gov/archive/nasa/casi.ntrs.nasa.gov/19980017535.pdf`.
[7] B. Montgomerie. Methods for Root Effects, Tip Effects and Extending the Angle of Attack to +/- 180 with Application to Aerodynamics for Blades on Wind Turbines and Propellers. Technical report, Swedish Defence Research Agency Scientific Report, FOI-R–1305–SE, 06 2004.
[8] Donghun Park, Yunggyo Lee, Th Cho, and Cheolwan Kim. Design and performance evaluation of propeller for solar-powered high-altitude long-endurance unmanned aerial vehicle. *International Journal of Aerospace Engineering*, 2018:1–23, 08 2018. doi: 10.1155/2018/5782017.
[9] Ohad Gur and Aviv Rosen. Multidisciplinary design optimization of a quiet propeller. In *14th AIAA/CEAS Aeroacoustics Conference (29th AIAA Aeroacoustics Conference)*, page 3073. AIAA, 2012. doi: 10.2514/6.2008-3073.
[10] Ohad Gur and Aviv Rosen. Optimizing electric propulsion systems for unmanned aerial vehicles. *Journal of Aircraft*, 46(4):1340–1353, 2009. doi: 10.2514/1.41027.
[11] Ohad Gur and Aviv Rosen. Optimization of propeller based propulsion system. *Journal of Aircraft*, 46(1):95–106, 2009. doi: 10.2514/1.36055.
[12] L.J. Clancy. *Aerodynamics*. Pitman Aeronautical Engineering Series. Wiley, 1975. ISBN 9780470158371. URL `https://books.google.mv/books?id=zaNTAAAAMAAJ`.
[13] Dale Lawrence and Kamran Mohseni. Efficiency analysis for long duration electric mavs. In *Infotech@Aerospace*, page 7090. American Institute of Aeronautics and Astronautics, 2012. doi: 10.2514/6.2005-7090.
[14] H. Glauert. *The Elements of Aerofoil and Airscrew Theory*. Cambridge Science Classics. Cambridge University Press, 1983. doi: 10.1017/CBO9780511574481.

[15] J. Hernández and A. Crespo. Aerodynamic calculation of the performance of horizontal axis wind turbines and comparison with experimental results. *Wind Engineering*, 11(4): 177–187, 1987. ISSN 0309524X, 2048402X. URL `http://www.jstor.org/stable/43749310`.

[16] M Sriti and Younes El Khchine. Improved blade element momentum theory (bem) for predicting the aerodynamic performances of horizontal axis wind turbine blade (hawt). *Technische Mechanik. Scientific Journal for Fundamentals and Applications of Engineering Mechanics*, 38(2):191–202, 01 2018. doi: 10.24352/UB.OVGU-2018-028.

[17] C. Bak, J. Johansen, and P.B. Andersen. Three-dimensional corrections of airfoil characteristics based on pressure distributions. In *2006 European Wind Energy Conference and Exhibition*, pages 1–10. European Wind Energy Association (EWEA), 2006.

[18] Hsue-Shen Tsien. Two-dimensional subsonic flow of compressible fluids. *Journal of the Aeronautical Sciences*, 6(10):399–407, 1939. doi: 10.2514/8.916.

[19] Shengyi Wang, Derek B. Ingham, Lin Ma, Mohamed Pourkashanian, and Zhi Tao. Turbulence modeling of deep dynamic stall at relatively low reynolds number. *Journal of Fluids and Structures*, 33:191 – 209, 2012. ISSN 0889-9746. doi: 10.1016/j.jfluidstructs.2012.04.011.

[20] Alex Araújo and et al. An assessment of different turbulence models on a cfd simulation of air flow past a s814 airfoil. In *24th ABCM International Congress of Mechanical Engineering*, page 9. ABCM, 01 2017. doi: 10.26678/ABCM.COBEM2017.COB17-0306.

[21] O. Günel, E. Koç, and T. Yavuz. Cfd vs. xfoil of airfoil analysis at low reynolds numbers. In *2016 IEEE International Conference on Renewable Energy Research and Applications (ICRERA)*, pages 628–632, 2016. doi: 10.1109/ICRERA.2016.7884411.

[22] APC. Apc propeller performance data. `https://www.apcprop.com/technical-information/performance-data/`, 2020. Accessed: 2020-02-15.

[23] F.C. Dougherty. *TAIR: A Transonic Airfoil Analysis Computer Code*. NASA technical memorandum. Ames Research Center, 1981. URL `https://books.google.com.co/books?id=2eJCAQAAIAAJ`.

[24] J.B. Brandt, R.W. Deters, G.K. Ananda, and M.S. Selig. Uiuc propeller database. `http://m-selig.ae.illinois.edu/props/propDB.html`, 2015. Accessed: 2020-02-15.

[25] Chandra Tjhai. Developing stochastic model of thrust and flight dynamics for small uavs. Master's thesis, University of Minnesota, 2013.

[26] A. Betz. Schraubenpropeller mit geringstem energieverlust. mit einem zusatz von l. prandtl. *Nachrichten von der Gesellschaft der Wissenschaften zu Göttingen, Mathematisch-Physikalische Klasse*, 1919:193–217, 1919. URL `http://eudml.org/doc/59049`.

[27] E. Eugene Larrabee. Practical design of minimum induced loss propellers. *SAE Transactions*, 88:2053–2062, 1979. ISSN 0096736X, 25771531. URL `http://www.jstor.org/stable/44699041`.

[28] Sydney Goldstein. On the vortex theory of screw propellers. *Proceedings of the Royal Society of London. Series A, Containing Papers of a Mathematical and Physical Character*, 123(792):440–465, 1929. ISSN 09501207. URL `http://www.jstor.org/stable/95206`.

[29] Umunna J Reuben, Koju Hiraki, and Miyamoto Shohei. Airfoil considerations in the design of high performance, low reynolds number propellers. *International Journal of Research - GRANTHAALAYAH*, 6(9):373–384, 2018.

[30] Airfoil tools. `http://airfoiltools.com/`, 2020. Accessed: 2020-02-15.